Model flames in the Boussinesq limit: The case of pulsating fronts

N. Vladimirova and R. Rosner*
ASC Flash Center, Department of Astronomy and Astrophysics, The University of Chicago, Chicago, Illiuois 60637, USA
(Received 28 September 2004; published 29 June 2005)

We extend earlier work on the nonlinear behavior of premixed flames in a gravitationally stratified medium, subject to the Boussinesq approximation, in two dimensions. The main result is that the nature of the traveling burning front is largely determined by the form of the adopted boundary conditions on the side walls: while symmetric boundary conditions lead to stably scalloped traveling wave solutions, loss of symmetry leads to the development of pulsating fronts. However, despite differences in geometrical features, the symmetric and asymmetric systems obey the same scaling behavior for the average effective flame speed.

DOI: 10.1103/PhysRevE.71.067303 PACS number(s): 47.70.Fw, 47.20.Bp, 47.55.Hd, 44.25.+f

The Boussinesq model is the simplest system exhibiting buoyancy effects without introducing the complexities associated with the presence of sound waves and gravitational stratification of the ambient medium. In our earlier article [1], we have studied flames in the Boussinesq limit in a two-dimensional Rayleigh-Taylor configuration (see also [2]). The heavier reactant was placed on top of the lighter product, with the interface between the reactant and the product slightly perturbed. The reaction front becomes Rayleigh-Taylor unstable, increasing the length of the interface and, consequently, the bulk burning rate. Eventually the front stabilizes in a "scalloped" shape, which propagates as a two-dimensional traveling wave. The shape of the interface and the traveling wave speed are determined by the maximum allowable wavelength and, in the limit of large wavelengths, are independent of the laminar flame speed.

The focus of [1] was on a comparison with classic single-mode Landau-Darrieus and Rayleigh-Taylor instabilities, and with the recent analytical results presented in [3]. We extended this study to systems with a multimode initial perturbation in [4], which required two modifications in the numerical setup. First, to initiate wrinkling of a planar interface, we added noise to the reaction rate. The noise did not influence the shape and the traveling wave speed of previously obtained scalloped solutions. Second, instead of considering half-wavelength computational domains with reflection boundary conditions at the vertical walls, we implemented periodic boundary conditions in the horizontal direction. To our surprise, the same calculations repeated in the one-wavelength domain (but with periodic boundary conditions) produce solutions with a very different character: instead of traveling waves, we now observe pulsating fronts. The difference in the nature of the solutions is apparently a result of the less restrictive conditions imposed on the transverse (horizontal) velocity.

The purpose of this report is to focus on the effects of boundary conditions in determining the asymptotic nature of the flame solutions. As the present work is an extension of [1], we discuss the results immediately after a short description of the model, and refer the reader to [1] for the details of the numerical method.

The Boussinesq model for combustion corresponds to the limit of an infinitely small density difference between burned and unburned states. The flow is assumed to be incompressible; the fluid crossing the interface does not undergo thermal expansion; and the reaction does not directly affect the velocity. A planar reaction front propagating with constant speed in a motionless fluid is a valid solution in a Boussinesq system. The scalar variable describing the reaction progress can be interpreted as temperature, scaled between zero and one, $0<T<1$. In the same spirit, we refer to a planar reaction front propagating in motionless fluid as a laminar flame.

The evolution of the temperature is described by an advection-reaction-diffusion equation, which is coupled to the fluid motion through the advection velocity. The fluid velocity obeys the incompressible Navier-Stokes equation with a temperature-dependent force term, $\mathbf{f}=\bar{\rho}\mathbf{g}(1-2AT)$. Here, $\mathbf{g}$ is the gravitational acceleration, $\bar{\rho}$ is the (constant) average density, and $A\equiv\Delta\rho/2\bar{\rho}$ is the Atwood number.

The governing equations are the 2D incompressible Navier-Stokes equation expressed in the vorticity formulation ($\omega\equiv\boldsymbol{\nabla}\times\mathbf{v}=-\nabla^2\psi$) and the advection-reaction-diffusion equation for the temperature:

$$\frac{\partial\omega}{\partial t}+(\mathbf{v}\boldsymbol{\nabla})\omega=\nu\nabla^2\omega+2Ag\frac{\partial T}{\partial x}, \tag{1}$$

$$\frac{\partial T}{\partial t}+(\mathbf{v}\boldsymbol{\nabla})T=\kappa\nabla^2T+\frac{1}{\tau}R(T), \tag{2}$$

$$\boldsymbol{\nabla}\mathbf{v}=0,$$

Where, κ is the thermal diffusivity, ν is the kinematic viscosity, τ is the reaction timescale, and g is the absolute value of the gravitational acceleration (which is assumed to be vertical). Note that the Atwood number and the gravitational acceleration appear only in the algebraic combination Ag for a Boussinesq system.

The reaction rate, $R(T)$, is typically some simple function of the temperature; however here we add a stochastic component, i.e.,

*Also at Enrico Fermi Institute, and Department of Physics, The University of Chicago, Chicago, IL 60637.

$$R(T) = \frac{1}{4}T(1-T)[1+\epsilon r(\mathbf{x},t)], \tag{3}$$

where $\epsilon \ll 1$ is the amplitude of the noise. The function $r(\mathbf{x},t)$ represents white noise; in our implementation r is a number chosen randomly within the interval $[-1,1]$ every time the reaction rate is computed. When $\epsilon=0$, the reaction rate reduces to the form used in [1]. As we show below, scalloped solutions are stable in systems with reflection boundary conditions and are metastable in systems with periodic boundary conditions. We use noise in reaction rate (3) to verify the stability in the first case and, in the second case, to reduce the time spent by the system in the metastable state (i.e., to speed up the calculations).

The thermal diffusivity and reaction time scale determine the laminar flame speed $s_0=\sqrt{\kappa/\tau}$ and the length scale $\delta=\sqrt{\kappa\tau}$. Because we use a diffuse representation of the flame, the reaction front has a finite thickness, of the order of δ. There is no universally accepted definition for the flame thickness; one possibility is to define it as a distance between two level sets, for example $T=0.1$ and $T=0.9$. Measured this way, the laminar flame thickness was found to be $\sim 18\delta$.

Our system is characterized by three nondimensional parameters: the Prandtl number, $\mathrm{Pr} \equiv \nu/\kappa$, the ratio of the perturbation wavelength to the flame length scale, $L \equiv l/\delta$, and the nondimensionalized gravity, $G \equiv 2Ag\delta/s_0^2$.

The case when $L \gg 1$, called the thin flame limit, is of special interest. In this limit the system behavior is determined by fluid flow on the large scales and is independent of choice of reaction $R(T)$. In the Boussinesq case discussed in [1], the speed and the shape of the traveling wave in the thin front limit depend only on the product LG. The LG product can be interpreted as the inverse square of the Froude number, $LG=\mathrm{Fr}^{-2}=2Agl/s_0^2$, where the Froude number is defined as the ratio of the laminar flame speed to the Rayleigh-Taylor velocity.

The initial conditions for most of our calculations are comprised of a quiescent velocity field (hydrostatic equilibrium) and an initially planar horizontal interface separating the unburned fluid above from the burned fluid below. A level of noise given by $\epsilon=10^{-2}$ is used in most of the simulations.

We performed simulations in two kinds of computational domains—a vertical channel of width $l/2$ with horizontally reflecting boundary conditions, and a vertical channel of width l with horizontally-periodic boundary conditions. For reflection boundary conditions the results are the same as obtained without noise in [1]: the system develops a stable, scalloped flame, propagating as a traveling wave. The system with periodic boundary conditions instead develops a pulsating front (Fig. 1).

The early development of a pulsating front looks very similar to the early development of a traveling wave. Indeed, by reducing the amount of noise we were able to observe traveling waves in the periodic system as well. However, these solutions do not represent the asymptotic behavior. The front maintains its scalloped shape only for a finite period of time (which could be substantial, when measured in units of the flame crossing time). Eventually the solution loses its symmetry and begins to pulsate; these pulsations subsequently persist. Thus, the scalloped solutions which are stable in the systems with reflection boundary conditions appear to be metastable in systems with periodic boundary conditions.

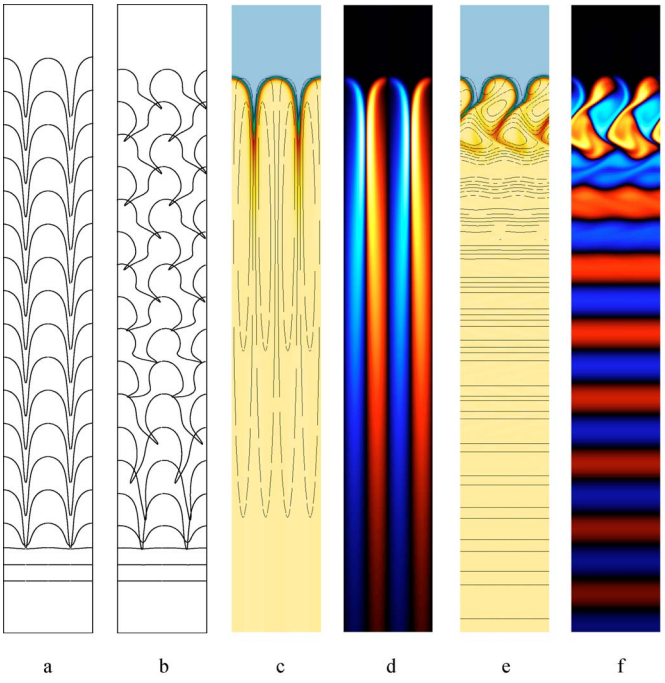

FIG. 1. (Color online). Panels A and B: the temporal development of the level set $T=0.5$, displayed at successive times separated by time intervals $\Delta t=25\tau$; panel A pertains to the case of reflecting boundary condition (the actual domain is replicated four times), while panel B pertains to the case of periodic boundary conditions (the domain is replicated twice). Panels C–F: the temperature distribution and velocity streamlines (panels C and E) and the vorticity distribution (panels D and F) at time $t=900\tau$ for same two cases. Simulation parameters: $L=64, G=1$, and $\mathrm{Pr}=1$.

The final, time-dependent behavior is asymptotic in the time-averaged sense, and is independent of the level of noise and the initial shape of the interface. Further on, we focus on the properties of this asymptotic state for the both systems, with periodic and reflection boundaries.

The difference between traveling waves and pulsating fronts originates in the vorticity distribution near and behind the flame front. As one can see from Eq. (1), vorticity is generated by the temperature gradients, e.g., at the flame interface. The sign of vorticity generated depends on the slope of the interface: positive vorticity is produced on the left sides of flame fingers, and negative on the right sides (see vorticity images in Fig. 1). The vorticity created at the flame front is advected into the burned material at the cusps, and ultimately dissipated well behind the flame front.

Reflective boundary conditions prohibit transverse horizontal velocities at the domain boundaries. The boundaries then act as separatrices between regions of positive and negative vorticity; and annihilation of vorticity of opposite signs occurs only as a result of viscous dissipation at the separatrices. Hence, the vorticity distribution takes the form of long vertical stripes, slowly fading out as one moves away

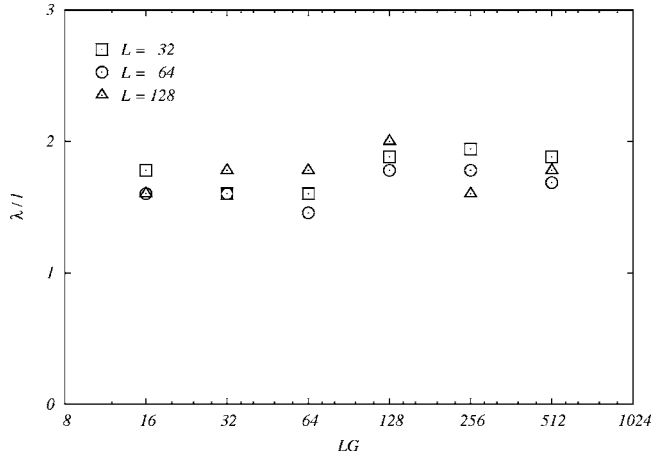

FIG. 2. Variation of the wavelength λ of horizontal shear vs the *LG* product in simulations with periodic boundary conditions for Pr=1 and three values of *L*. The striking result is the insensitivity of this shear scale to the *LG* product, which is otherwise a key control parameter for this problem.

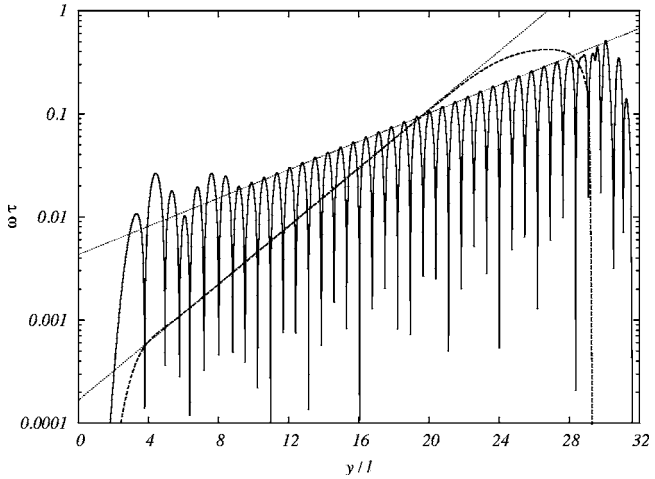

FIG. 3. Absolute value of the nondimensionalized, horizontally averaged vorticity as a function of height for a system with $L=64, G=1$, and Pr=1, with periodic boundary condition (solid) and with reflection boundary conditions (dashed). The slopes of the two dotted lines correspond to the vorticity dissipation rate computed using Eq. (4) with average flame speed $s/s_0=1.900$ and $s/s_0=1.859$, respectively, and $\lambda/l=1.45$.

(e.g., down) from the flame interface. Correspondingly, the velocity field consists of pairs of horizontal counter-rotating rolls that are elongated in the vertical direction. Because of this elongation, the flow along the separatrices can be regarded as a shear flow along the vertical direction.

In contrast, if the boundary conditions are periodic, transverse velocities at the boundaries are allowed. As a consequence, a horizontal shear flow can, and does, develop. This shear distorts the reaction front; the vorticity is deposited in an asymmetric pattern, which leads to horizontal stripes of alternating positive and negative vorticity in the wake of the propagating flame front. The vertical component of the velocity is dissipated by diffusion behind the burning front, resulting in layers of oppositely signed vorticity. These layers are stationary and regularly spaced, and are characterized by a vertical wavelength λ discussed further below. The layers interact with one another only through diffusion, and eventually dissipate well behind the flame front.

The frequency of pulsations depends on gravity *G* and horizontal wavelength *L*, but the vertical wavelength λ, which is a ratio of the average flame speed to the frequency, is surprisingly invariant. We measured λ for a wide range of parameters and various initial conditions, and found that the ratio of the vertical to horizontal wavelengths is roughly constant (Fig. 2). However, the uncertainty in this measurement remains relatively large, and a slight dependence on control parameters cannot be ruled out. The results for different Prandtl numbers are not shown in Fig. 2, but they follow the same trend (no significant dependence of λ on Prandtl number).

In spite of the dramatic differences in geometrical and temporal features of the underlying flows, the two classes of solutions (steady scalloped fronts and pulsating fronts) have similar mechanisms of vorticity dissipation behind the flame. In both cases, vorticity decay is dominated by high frequency modes $\Delta\omega/\omega=-\nu k^2\Delta t$, where $k=k_x=2\pi/l$ for vertical shear, and $k=k_y=2\pi/\lambda$ for horizontal shear. We can also estimate the decay rate of vorticity by assuming exponential decay on a length scale h_V, e.g., $\Delta\omega/\omega=\Delta y/h_V$, where the displacement Δy equals to the shift of the solution during the time interval, $\Delta y=s\Delta t$, where *s* is the traveling wave speed. We thereby estimate the vorticity dissipation length scale

$$h_V=\frac{s}{\nu k^2}. \tag{4}$$

To summarize, the vorticity well behind the flame can be approximated by the expression,

$$\omega=\omega_0\cos(\mathbf{k}\cdot\mathbf{x})e^{(y-st)/h_V}, \tag{5}$$

with $\mathbf{k}=(2\pi/l,0)$ for the vertical shear, and $\mathbf{k}=(0,2\pi/\lambda)$ for the horizontal shear, cases. Although Eq. (5) does not exactly satisfy Eq. (1), it does demonstrate excellent agreement with our numerical results; we indicate this agreement in Fig. 3 by comparing the horizontally averaged computed vorticity and the vorticity dissipation rate, as estimated by using Eqs. (4) and (5). Note that the vorticity dissipation length scale is a function of the effective flame speed, which in turn is a function of gravity.

Finally, we discuss the relationship between flame morphology and the effective flame speed. In a similar two-dimensional numerical setup, Bayliss *et al.* [2] observed flame behavior ranging, as the effective flame speed increases, from planar flames, to steady scalloped flames, to pulsating fronts, and finally, to chaotic flames.

The transition between planar and scalloped flames occurs when the gravity parameter exceeds some critical value, $G_{cr}=G_{cr}(L)$. For values of *G* below critical, the scalloped solution does not exist, and the traveling wave has a planar interface moving with the laminar flame speed s_0. For values of *G* above critical, Pr=1, and reflective boundary conditions, we observed the scaling

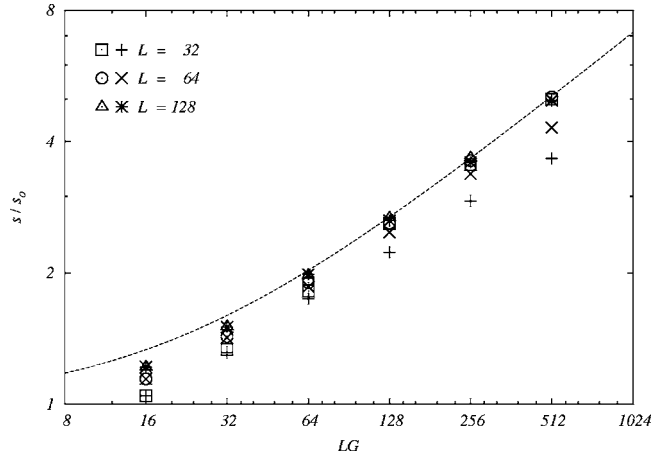

FIG. 4. Average flame speed to laminar flame speed ratio as a function of the LG product, for $L=32$, $L=64$, $L=128$, and $\mathrm{Pr}=1$, for a system with reflecting boundary conditions (open symbols) and with periodic boundary conditions (crosses). The dashed curve corresponds to Eq. (6)

$$s = s_0\sqrt{1 + \alpha L(G - G_{\mathrm{cr}})}, \tag{6}$$

where $\alpha \approx 0.0486$ is constant [1].

When we consider periodic boundary conditions, we find that the time dependence and symmetry properties of the flame have no influence on the transitional behavior and on the flame speed for values of gravity below and moderately above critical (Fig. 4). Inspection of the flame front reveals that the flow at the flame tips resembles the counter-rotating vortices typical for a rising bubble and seen in the scalloped front regime. Since the front is only slightly curved for small values of LG, the horizontal shear either develops below the flame brush (for large values of L) or is weakened by dissipation (for small values of L). In both cases, the shear distorts the flame front in the lower, mostly burned layer of the flame brush, leaving the tips unaffected (Fig. 1). This regime can be interpreted as a stable scalloped front in [2].

As the LG product increases, the influence of periodic boundary conditions on flame morphology becomes more noticeable. Underlying shear bends the flame fingers closer to the tips, the interface area shrinks and extends periodically, and the flame speed begins to oscillate, i.e., the flame front pulsates.

With further increase of LG, the oscillation pattern becomes more complicated and takes longer to settle down to a coherent pulsating state, suggesting a possible transition to chaotic flames as described in [2].

However the boundary conditions and complicated flame front behavior do not affect the average flame speed for sufficiently large values of L. Expression (6) was obtained for a thin flame regime, which requires not only $L \gg 1$, e.g., a thin laminar flame, but also small flame thickness when the flame is distorted by the flow. The vertical shear flow better preserves the structure of long vertical channels of unburned fluid near the separatrices where significant fraction of the burning occurs, while horizontal shear flow is more likely to destroy those channels. As a result, the flame speed for $LG \gg 1$ and $G > 1$ is lower than suggested by Eq. (6) in a system with periodic boundary conditions.

Note that in the large LG limit the effective flame speed does not depend on a laminar flame speed, $s \propto s_0\sqrt{LG} = \sqrt{2Agl}$. This has been observed in both numerical simulations and in experiments of flames rising in tubes (see review, [5]), as well as in fully compressible simulations using periodic boundary conditions both in two and three dimensions [6,7]. Indeed, flames in tubes develop traveling wave solutions with smooth fronts, while flames in periodic systems develop complicated nonstationary interfaces [5].

This work was supported by the Department of Energy under Grant No. B341495 to the Center for Astrophysical Thermonuclear Flashes at the University of Chicago.

[1] N. Vladimirova and R. Rosner, Phys. Rev. E **67**, 066305 (2003), and references therein.
[2] A. Bayliss, T.-K. Ma, and B. J. Matkowsky, SIAM J. Appl. Math. **61**, 1103 (2000).
[3] P. Constantin, A. Kiselev, and L. Ryzhik, Commun. Pure Appl. Math. **56**, 1781 (2003).
[4] N. Vladimirova *et al.* (in preparation).
[5] V. V. Bychkov and M. A. Liberman, Phys. Rep. **325**, 115 (2000).
[6] A. M. Khokhlov, Astrophys. J. **449**, 695 (1995).
[7] O. E. B. Messer *et al.* Astrophys. J. (submitted).